LRP 344/88 March 1988

The Phase Contrast Method as an Imaging Diagnostic for Plasma Density Fluctuations

H. Weisen

Invited Paper presented at the

7th TOPICAL APS CONFERENCE ON HIGH TEMPERATURE PLASMA DIAGNOSTICS
Napa, California
March 13-17, 1988

THE PHASE CONTRAST METHOD AS AN IMAGING DIAGNOSTIC FOR PLASMA DENSITY FLUCTUATIONS

H. Weisen

Centre de Recherches en Physique des Plasmas
Association Euratom - Confédération Suisse
Ecole Polytechnique Fédérale de Lausanne
21, Av. des Bains, CH - 1007 Lausanne / Switzerland

ABSTRACT

An imaging diagnostic for the observation of plasma density fluctuations is presented. It is based on the phase contrast method, and is used on the TCA tokamak to investigate fluctuations associated with plasma turbulence and driven waves in radio frequency heating experiments. The diagnostic uses a 23 cm wide CO_2 laser beam transmitted through the plasma, and produces an image of the plasma where the small phase shifts ($|\phi| \sim 10^{-5}$ to 10^{-3}) due to refractive perturbations are revealed as corresponding intensity variations. A wide range of fluctuation wavelengths between 0.2 and about 20 cm is accessible to observation, with a sensitivity better than 10^{-5} radians for a 1 MHz bandwidth.

INTRODUCTION

Electron density fluctuations, such as those associated with plasma turbulence, are traditionally investigated using microwave or infrared scattering techniques.[1]

The scattered radiation is detected in the far field where it is resolved in its wavenumber components. Alternatively the scattered light can be detected in the near field,[2] or at an image of the scattering volume (or plasma) provided by a suitable optical arrangement.[3,4] In this case the scattered light is spatially rather than wavenumber resolved.

In principle, the two approaches are equivalent, the same scattered power and the same information being available in the near and the far field of the scattering volume. In a finite laboratory plasma, however, far field diagnostics can be handicapped by the requirement that the scattering volume should be small enough to provide a homogenous plasma sample, and simultaneously large enough for adequate wavenumber resolution. When the spatial scales of the fluctuations and the scales over which the plasma can be considered to be homogenous are not clearly separable, imaging diagnostics have the advantage of providing the information in its natural spatial representation. This will be the case for long wavelength turbulence,[5] MHD instabilities, and complicated or localised wavepatterns as observed during Alfvén Wave Heating in TCA.[6]

When the scales of the density fluctuations are sufficiently large, corresponding to the regime of Raman-Nath diffraction,[7] the effect of the fluctuations on the transmitted wave is described by the usual eikonal phase $\phi(\underline{x},t)=k_0\int n(\underline{x},z,t)dz$, where k_0 is the probe wavenumber, n the plasma refractive index, and z direction of propagation. Its measurement is most naturally performed by interferometry or a related method, like phase contrast. Whereas the interferometer uses a reference beam external to the plasma, the phase contrast method relies on deriving an "internal reference" from the transmitted beam. This renders the phase contrast device considerably less sensitive to mechanical perturbations than an interferometer, making a rigid C-frame unnecessary. At the same time a substantial sensitivity

enhancement over interferometry is achieved by the spatial filtering process involved.

The phase contrast method was invented in 1934 by the Dutch physicist Zernike and first applied to microscopic observation.[7,8] It has to our knowledge only been applied by one group to investigate plasmas of fairly high density ($n_e > 10^{16} cm^{-3}$) using a pulsed ruby laser.[9]

In the basic setup (Fig. 1) a collimated monochromatic beam is transmitted through the refractive object centered at the plane Σ and the focussed by lens L_1 onto a so called phase plate (or phase mirror if it is a reflective device) P where it is resolved in its wavenumber spectrum. The undiffracted light (corresponding to diffraction order 0) is focussed onto the central depression on P (called conjugate area), whereas light diffracted by the refractive object (into orders +1 and -1) intersects the plate beside it (at the complementary area). The depth of the depression is designed to introduce a $\pi/2$ phase shift upon transmission between the diffracted and the undiffracted components. Lens L_2 then recombines these components in the image plane Σ. In the Raman-Nath regime, where the wavenumber spectra are symmetrical, the $\pi/2$ phase shift is essential to obtain measurable interference in Σ between the diffracted light components and the much larger undiffracted part which serves as a reference or local oscillator. The intensity of this homodyne local oscillator can be controlled by a suitable choice of the transmittance γ of the conjugate area. (Heterodyne versions have also been proposed[10]).

For an incident plane wave B(x,t) of unit amplitude, the amplitude transmitted through the object can be written as

$$B'(\underline{x},t) = \exp(i\phi(\underline{x},t)) \cong 1 + i\phi(\underline{x},t) \text{ for } |\phi| \ll 1.$$

As a result of the spatial filtering described above, the complex amplitude in the image plane is

$$B''(\underline{x},t) \cong \gamma + \phi(\underline{x},t),$$

and the intensity for first order in ϕ is

$$I(\underline{x},t) = |B''(\underline{x},t)|^2 \cong \gamma^2 + \gamma\phi(\underline{x},t) \qquad (1)$$

In a real device the conjugate area must be at least as wide as the diffraction limited focal spot size at P, and only diffracted light falling onto the complementary area can contribute to the

interference term in Eq. (1). Thus the instrument is a spatial high pass device, with a cutoff wavenumber $k_c \geq 2\pi/D$, where D is the beam diameter.

I. TRANSFER PROPERTIES AND SENSITIVITY

If B(x) describes the probe beam complex amplitude profile, the transmitted beam B'(x) becomes (dropping the temporal dependence and vector notation for convenience)

$$B'(x) = [1+ i\phi(x)]B(x) \text{ for } |\phi| \ll 1. \tag{2}$$

The amplitude in the focal plane is a scaled version of the Fourier transform of B(x),

$$\tilde{B}'(k) = [\delta(k)+i\tilde{\phi}(k)] \otimes \tilde{B}(k) \tag{3}$$

where a tilde designates a Fourier transform and $\otimes$ the convolution operation. The effect of the phase plate can be described by

$$\tilde{B}''(k) = [1-\tilde{C}(k)+i\gamma\tilde{C}(k)]\tilde{B}'(k), \tag{4}$$

where $\tilde{C}(k)$ is the characteristic function of the conjugate area extending from $-k_c$ to k_c. $\tilde{C}(k)$ takes the value 1 inside this interval and 0 outside. γ is the amplitude transmittance of the conjugate area ($\gamma \leq 1$). Neglecting the magnification m=f2/f1 the inverse transform of (4) provides the complex amplitude B"(x) and intensity I(x) in the image plane:

$$B''(x) = R(x)+D(x) \tag{5}$$
$$R(x) = (i\gamma-1)B(x)\otimes C(x) + B(x)$$
$$D(x) = i\phi(x)B(x) - (\gamma+i)[\phi(x)B(x)]\otimes C(x)$$
$$I(x) = |R(x)|^2 + |D(x)|^2 + R^*(x)D(x) + D^*(x)R(x) \tag{6}$$

The two last terms of Eq. (6) describe the linear intensity variation caused by the presence of the phase shift $\phi(x)$. Properly

focussing and centering the direct light ($\tilde{B}(k)$) at the phase plate amounts to considering B(x) a real function in the above equations, thus

$$\Delta I(x)=R^*(x)D(x) + D^*(x)R(x)$$
$$=2\gamma\, B(x)\, \{[B(x) \otimes C(x)]\, \phi(x) - [\, \phi(x)\, B(x)] \otimes C(x)\} \qquad (7)$$

For a given point x_0 in Σ, $\Delta I\,(x_0)$ is essentially proportional to the difference between $\phi(x_0)$ and a weighted average of $\phi(x)$ over the neighbourhood of x_0.

This feature suggest the designation "internal (or floating) reference interferometer" for the phase contrast device. It has been shown that in a conceptually ideal internal reference interferometer the weighting function is just the normalised intensity profile ($|B(x)|^2$) of the probe beam.[4] When the size of the conjugate area is closely matched to the diffraction limited spot size, then the weighting function for phase contrast, which is proportional to $B(x)\ C(x-x_0)$, can closely approach this ideal limit. Replacing $\phi(x)$ by $\delta(x-x_0)$ in Eq. (7) we obtain the impulse response of the system

$$h(x,x_0) = 2\,\gamma\, I_0(x)\ \{\ \delta(x-x_0) - \frac{B(x_0)\ C(x-x_0)}{B(x) \otimes C(x)}\ \} \qquad (8)$$

where $I_0(x) = B(x)[B(x) \otimes C(x)]$. For x fixed, a Fourier transform on the variable $(x-x_0)$ of $h(x,x_0)$ provides a local wavenumber response function. For, e.g., x=0, it becomes

$$H(k) = 2\,\gamma\, I_0\ \{1 - \frac{\tilde{B}(-k) \otimes \tilde{C}(k)}{\tilde{B}(-l) \otimes \tilde{C}(l)\ |_{l=0}}\ \} \qquad (9)$$

The behaviour of H(k) is sketched on Fig. 2, for the representative case where B(x) is even. For $k>k_c$, the response of the system becomes wavenumber independent.

When the object is located at some distance z from Σ, i.e. is out of focus, the wavenumber response of Eq. (9) has to be multiplied by the factor $\cos(zk^2/2k_0)$. The requirement that this correction should be small defines an allowable depth of field, which for $\lambda = 10.6\mu$ will extend over the whole plasma for

perturbations with 1 cm wavelength even in the largest existing fusion research devices.

When photodetectors such as photovoltaic diodes or photoconductive elements are used to probe the image plane, and the local oscillator intensity $\gamma^2 I_0$ is sufficient, sensitivity is only limited by shot noise from the local oscillator photocurrent. The signal to noise power ratio (for k>kc), then is

$$S/N = 2\, A\eta I_0 \langle\phi^2\rangle (h\upsilon\Delta f)^{-1} \qquad (10)$$

where A is the sensitive area, η the quantum efficiency, $h\upsilon$ the photon energy and Δf is the bandwidth. In many cases, S/N is limited not by the available laser power, but by saturation of the detectors by the local oscillator power $I_{lo} = \gamma^2 I_0$, i.e. constraining Eq. (10) by the condition $I_0 < \gamma^{-2} I_{sat}$. Thus in practice sensitivity limits for ϕ scale like γ^{-1}, whence the interest of the contrast enhancement achieved by reducing the transmittance of the conjugate area.

II. OPTICAL ARRANGEMENT ON THE TCA TOKAMAK

The optical system shown in Fig. 3 can be divided into three parts which are namely the beam production optics mounted on the rear of the vertical optical table (PL), the beam transport optics consisting of flat relay mirrors (MR) and composite NaCl vacuum windows[12] (F), and the imaging and detection optics on the front side of PL. The beam from an 8-Watt CO_2 waveguide laser (λ=10.6μ) is expanded to a width of 23 cm (1/e of intensity), then relayed to the plasma and imaging optics (Fig. 4) by six mirrors MR (45x7 cm in size) mounted three by three at right angles to each other in two rigid boxes. The upper box is mounted to the tokamak support structure, whereas the lower one stands on the floor. The boxes and the optical plate are independently vibration isolated with simple rubber or foam pads. Thanks to the corner-cube arrangement of the relay mirrors the system is insensitive to rigid body movements of any of these three subunits. This ascertains stable focussing onto the phase mirror (MP) by the

paraboloid P (f=190.5 cm) even in the presence of strong mechanical perturbations during plasma discharges.

Phase mirrors were made by coating flat steel mirrors with a 1.4μ thick Al-layer while thin brass ribbons of suitable width (120 -1030μ for a spot size of about 120μ) were stretched across them as masks. At an incidence of 20° they produce the desired $\pi/2$ phase-shift between undiffracted light reflected from the bottom of the groove and diffracted light reflected from the coating. The conjugate area is oriented to allow detection of perturbations having a wavenumber component perpendicular to the toroidal magnetic field ($k_\perp > k_c$). To further reduce the absorbtion of the direct beam the mirrors were overcoated with a layer of gold. Recently phase mirrors produced on ZnSe and BaF_2 substrates have been introduced to enhance the contrast ($\gamma^2 = .16$ and .04 respectively, Fig. 5).

The configuration and magnification of the imaging optics can be chosen very flexibly according to the specific tasks and the detectors available. In most of the earlier work single element HgCdTe detectors of sizes 0.25, 0.5 and 1 mm were used with magnifications in the range 1/5 to 1 and a resolution of the order of 1 mm.[5,6,10] The full potential of the diagnostic is, however, only exhausted with a detector array with tens of elements covering the available aperture. Figure 4 shows the arrangement of the imaging optics used for Alfvén Wave studies using a linear array of 30 photoconductive HgCdTe elements (250μ x 250μ, 50μ spacing). The overall magnification is 1/19, for a full coverage of the outer half of the plasma cross-section with 5.7mm resolution. The sensitivity limit is given by the saturation of the HgCdTe elements ocuring for $\eta I_{|0} \sim 1$ to 2 mW/mm^2. For the largest detectors the limit (S/N=1) obtained corresponds to $|\phi| \cong 2 \cdot 10^{-6}$ radians for a 1 MHz bandwidth, which is within a factor of two of the shot noise limit for $\eta I_{|0} = 1$ mW and $\gamma^2 = 0.16$. For effective integration lengths of a few cm this corresponds to a relative fluctuation level $\Delta n/n$ of a few times 10^{-5} under typical tokamak conditions.

III. PERFORMANCE TESTS AND CALIBRATION

Three different methods have been devised to measure the transfer characteristics of the phase contrast diagnostic. The most direct is to measure the response to sinusoidal perturbations such as sound waves produced by a loudspeaker directed transversely across the beam. The response measured has to be normalised to the sound pressure and to the effective integration length L, which depends on the acoustic wavelength $\Lambda=2\pi/k$, because the loudspeaker produces a spherical wavefield of the form $\Delta n(r,t) \alpha r^{-1} \exp[i(kr-\omega t)]$, where $r=(x^2+z^2)^{1/2}$. For $z \ll x$ the line integral of Δn can be evaluated analytically under the approximation $r \cong x(1+z^2/2x^2)$:

$$\phi(x,t) \alpha k_0 x^{-1} \exp[i(kx-\omega t+\pi/4)] \bullet \sqrt{2\pi x/k}. \qquad (11)$$

This approximation holds within less then 10% provided $x > 2\Lambda$. (The distance x between the loudspeaker and the viewing chord was 100 cm.) The sound pressure at the viewing chord was measured using a calibrated sonometer (Brüel & Kjaer model 2230). Figure 6 shows the normalized responses for two phase mirrors with conjugate area widths w of 200 and 1030 μ respectively. There is good agreement with the expected values for k_c and with the response expected from Eqs. (1) and (11) for the plateau at $k>k_c$. The latter is indicated for w = 1030 μ by the horizontal line and was obtained from the absolute sound pressure measurement Δp. It was related to the refractive index variation assuming adiabatic compression.

Another method is to measure the system's step response obtained by scanning a 12 μm thick sheet of MYLAR across the object plane. By a suitable choice of its inclination it produces phase steps of $2\pi\pm\varepsilon$ with ε ~0.1. Figure 7a shows an example of step response obtained for w=200 μ. The corresponding wavenumber response H(k), Fig. 7b was obtained by dividing the Fourier transform of the step response by the Fourier transform of the step. Here H(0) is non zero owing to the transmittance of about 85% of the Mylar sheet. (The phase contrast systems acts as a low pass filter for small variations of amplitude transmittance).

The third method, which is easily applicable only for $\gamma \cong 1$, allows a direct visualization of the system's impulse response. It consists in scanning an opaque bar of small dimensions across the object plane. At the position of the bar the intensity is approximately doubled. The decrease of intensity in the surroundings is proportional to the second right hand term in Eq. (8).[10] Figures 7c and d show the impulse and wavenumber responses obtained for w=200 μ. For all three methods there is good agreement between the measured cutoff k_c and the expected value $k_c = \pi w (f_1 \lambda)^{-1} \cos(20°)$.

The absolute sensitivity varies across the image plane for a single element detector and varies from element to element for the detector array. A calibration signal provided by a tweeter operating at 20 kHz is used to renormalize the raw signals from the plasma. In the case of the detector array, a multiplexer circuit scans the response from the 30 channels 50 ms prior to each tokamak discharge (Fig. 8a). The sound wave produced by the tweeter also provides an example of a wave propagation measurement (Fig. 8b). Note that phase contrast being a homodyne technique is no obstacle to the determination of the direction of propagation.

IV. APPLICATION TO THE TCA TOKAMAK

The main motivation for the development of this instrument was to study the wave physics underlying the principle of Alfvén Wave Heating (AWH) in the TCA tokamak (R=61cm, a=18cm, $B_T \leq 1.5T$, $I_p \leq 170kA$, $\bar{n}_e \leq 10^{14} cm^{-3}$, $T_e(0) \cong 800eV$).

In earlier work we had to rely on the reproducibility of the tokamak discharges to obtain radial profiles using a single scannable detector.[6] In our present system the signals from 16 channels of the 30 element array are synchronously amplified by two eight channel mixer arrays. The reference signal is derived from the pilot oscillator controlling the rf generator and is thus in phase with the current in the launch antennae. Prior to mixing the signals are bandpassed (1-4 MHz), for rf frequencies typically in the range 1.8-2.7 MHz. Post-mixing bandwidths are typically 1-10 kHz. The in-phase and quadrature components are acquired by two

16 channel ADC's.

The example of Fig. 9 shows the evolution of the amplitude of the synchronous density oscillations for 16 positions covering the range r/a=0 to 0.8. Also shown is the amplitude of a pick-up coil outside the limiter radius showing the occurence of two global resonances (DAW) attained in the course of the density rise.

The fluctuations observed after the first DAW correspond to the kinetic Alfvén wave (KAW) and are excited at the (n,m)=(2,0) resonance layer where $\omega/k_{||}=v_A$. Inspection of the phase profile reveals a radially inward propagating wave with a wavelength of a few cm (Fig. 10). Due to the shell-like radial structure of the KAW, local values of Δn can be obtained from the line integrated measurement using an effective integration length as already explained in section 3 for a spherical sound wave. During global resonances the fluctuations have the character of standing waves.

The instrument has also been used to investigate low frequency (f<1 MHz) broadband turbulence.[11] Wavenumber spectra were obtained from spatial Fourier transforms on the measured spatial correlation functions obtained using two scannable detectors. With the detector array spatial correlation functions are obtained in a single discharge even if only a modest number of fast ADC's are available. Figure 11 shows the spectral coherence and relative phase at 100 kHz (Δf=12 kHz) of the signals from element pairs as a function of relative separation Δx.

The signals of 8 elements were acquired using 8 available synchronised transient digitizers (Le Croy TR8837F). By selecting a suitable set of unevenly spaced elements (indicated in the figure) an almost continuous coverage of the possible separations was obtained, ranging from 0.33 cm to 9.7 cm. The overall magnification was 1/9 in this case. The figure shows that at the frequency of 100 kHz (corresponding to the maximum spectral power density) the coherence length and mean wavelength are about 4cm. This wavelength would already be too long to be adequately resolved by scattering diagnostics using beam widths of only 1or 2 cm.

In the case of turbulence the retrieval of local fluctuation levels from line measurements is difficult because symmetry assumptions are difficult to justify. Estimates are obtained using

an effective integration length given by the geometric mean of the correlation length and the size of the turbulent plasma.[11]

V. Conclusions

The phase contrast method, as exemplified by its applications to the TCA tokamak, is a very sensitive and versatile tool to investigate a broad range of plasma density fluctuations. Proposed applications other than those presented here include e.g. the observation of mode conversion processes during ICRH, magnetic islands, and various kinds of MHD modes and instabilities.

The construction and operation of imaging diagnostics with a large field of view is now facilitated by the existence of reliable commercial CO_2 lasers and infrared detector arrays, and the availability of generously dimensioned infrared window materials at affordable prices.

Acknowledgments

I would like to express my gratitude for a fruitful collaboration with my colleagues of the TCA Team and for the support of Dr. R. Behn and Prof. F. Troyon, as well as the assistance of the technical staff and secretaries at the CRPP. Thanks are extended to Dr. C.A.J. Hugenholtz, FOM Institute for Plasma Physics (NL), who generously lent us a 30 element detector array. This work was partly supported by the Swiss National Science Foundation.

References

1 see e.g.
- R.E. Slusher and C.M. Surko, Phys. Fluids 23, 472 (1980).
- H. Park, D.L. Brower, W.A. Peebles, N.C. Luhmann, R.L.Savage, and C.X. Yu, Rev. Sci. Instrum. 56, 1055 (1985).
- T. Crowley and E. Mazzucato, Nucl. Fusion 25, 507 (1985).

2 L.E. Sharp, Plasma Physics 23, 472 (1983).

3 H. Weisen, Infrared Physics 23, 543 (1985).

4 H. Weisen, Plasma Phys. Contr. Fusion 28, 1147 (1986).

5 H. Weisen, W. Simm, A. Pochelon, Ch. Hollenstein, and R. Behn, Plasma Phys. Contr. Fusion 28, 1161 (1986).

6 R. Behn, G.A. Collins, J.B. Lister, and H. Weisen, Plasma Phys. Contr. Fusion 29, 75 (1987).

7 see e.g. Born and Wolf, Principles of Optics, Pergamon Press (1959).

8 F. Zernike, Mitt. Naturkundig. Labor, Univ. Groningen, Physica, Haag 1, 43 (1934).

9 H.M. Presby and D. Finkelstein, Rev. Sci. Instrum. 38, 1563 (1967).

10 H. Weisen, Thesis No 659, Ecole Polytechnique Fédérale de Lausanne, 1986 (also CRPP Report LRP 312/86).

11 H. Weisen, Ch. Hollenstein, and R. Behn, Plasma Phys. Contr. Fusion, in press (1988) (also CRPP Report LRP 327/87).

12 H. Ripper and H. Weisen, Infrared Phys. 27, 375 (1987).

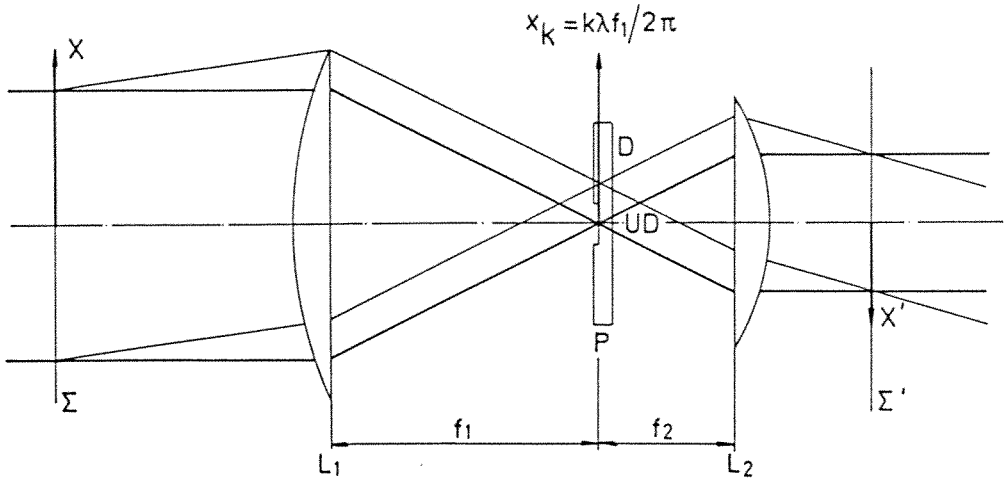

Fig. 1. Basic setup for phase contrast; Σ, object plane; Σ', image plane; P, phase plate; D, diffracted light component; UD, undiffracted light component; L_1 and L_2, focusing and imaging lenses.

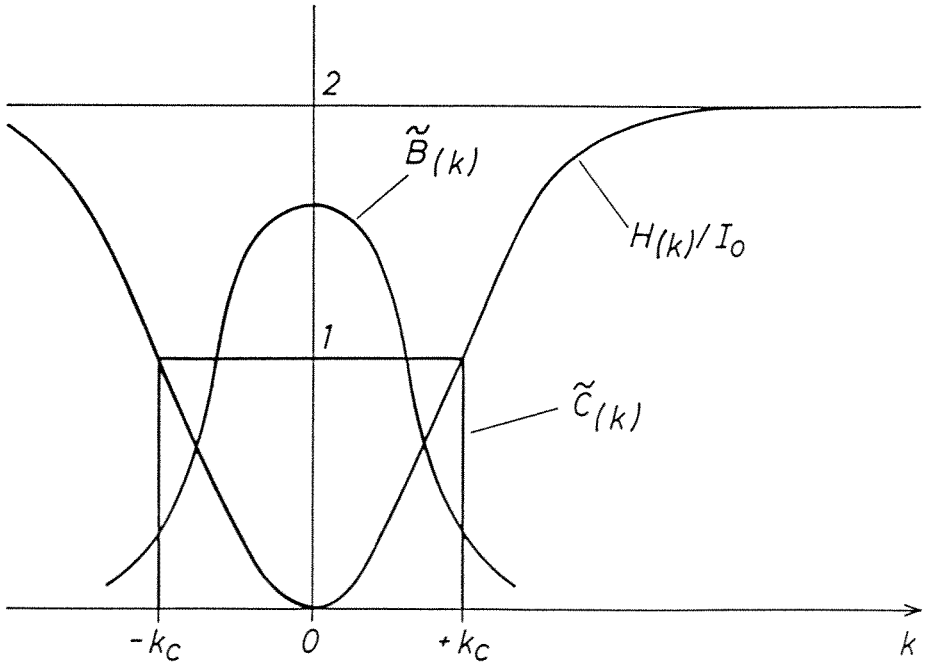

Fig. 2. Wavenumber response from Eq. 9.

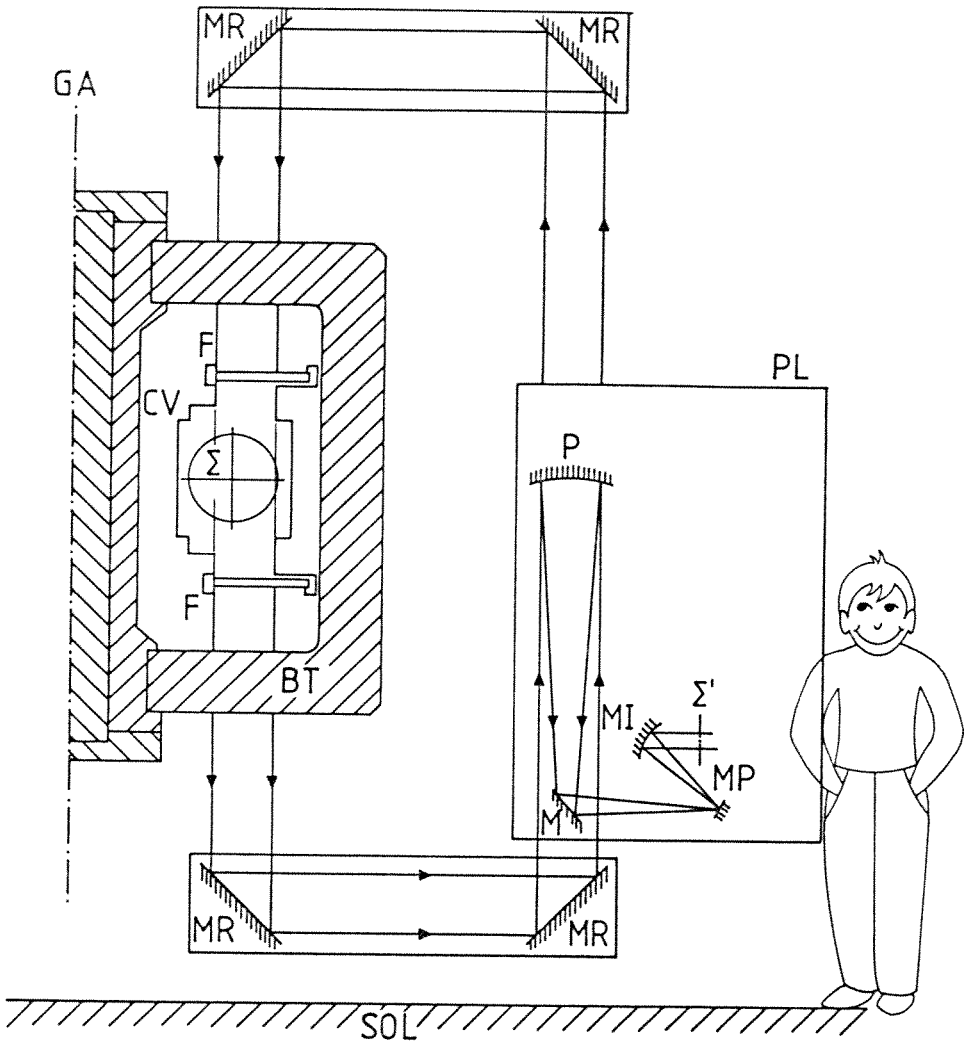

Fig. 3. Optical arrangement on the TCA tokamak
PL: optical table, P: parabolic mirror (f=190.5 cm), M: flat mirror, MP: phase mirror, MR: relay mirror, F: NaCl vacuum window, CV: vacuum chamber, BT: toroidal field coil, GA: major axis, Σ: object plane at plasma mid-plane, Σ': image plane (imaging optics simplified).

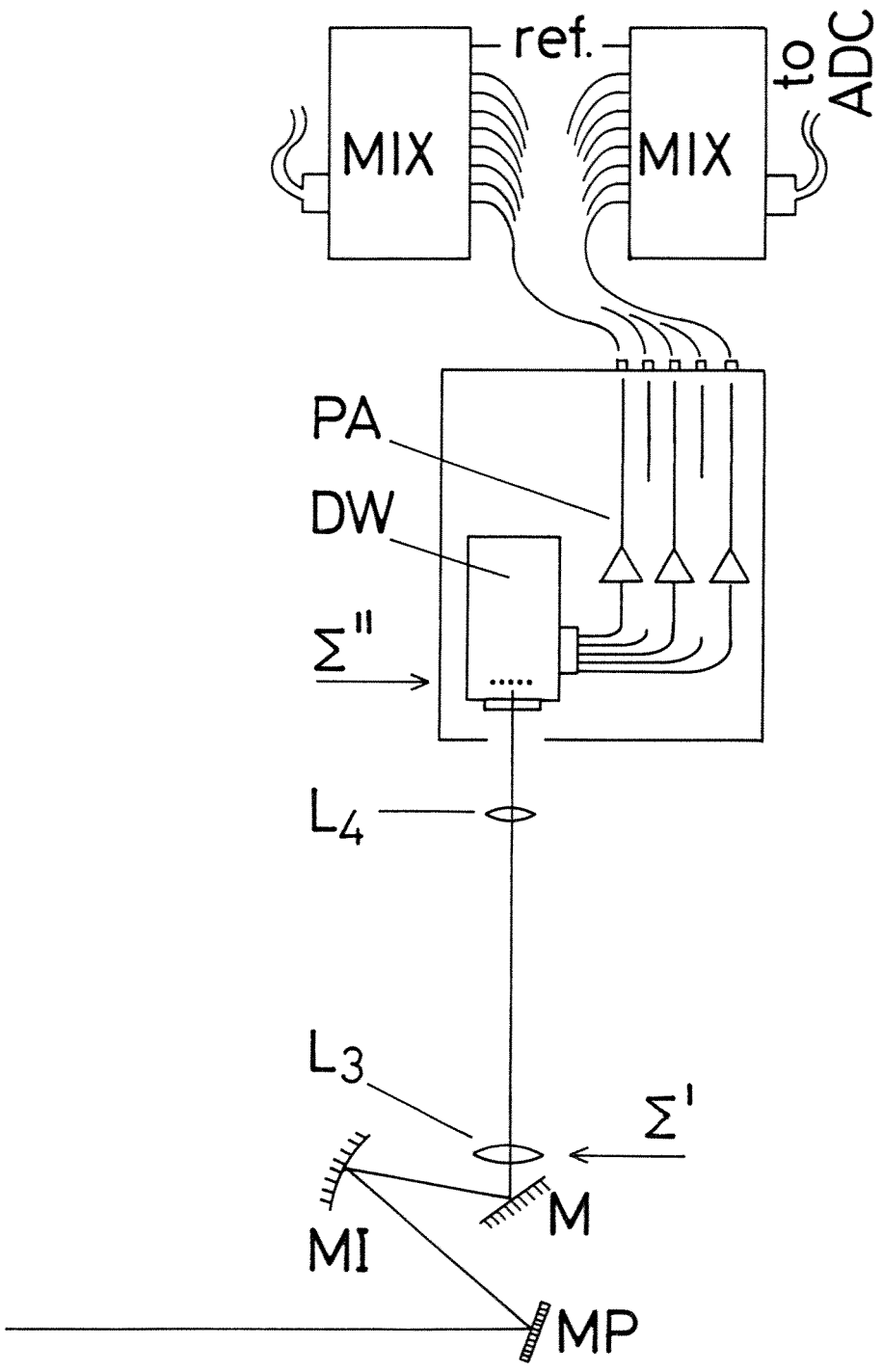

Fig. 4. Imaging optics: MP: phase mirror, MI: imaging mirror (f=27 cm), M: mirror, Σ': first image plane, L_3: field lens (f = 35 cm), L_4: second imaging lens (f=10cm), Σ'': second image and detection plane, DW: detector and dewar, PA: preamplifiers (x30, gain = 4000), MIX: eight channel mixers for synchronous detection.

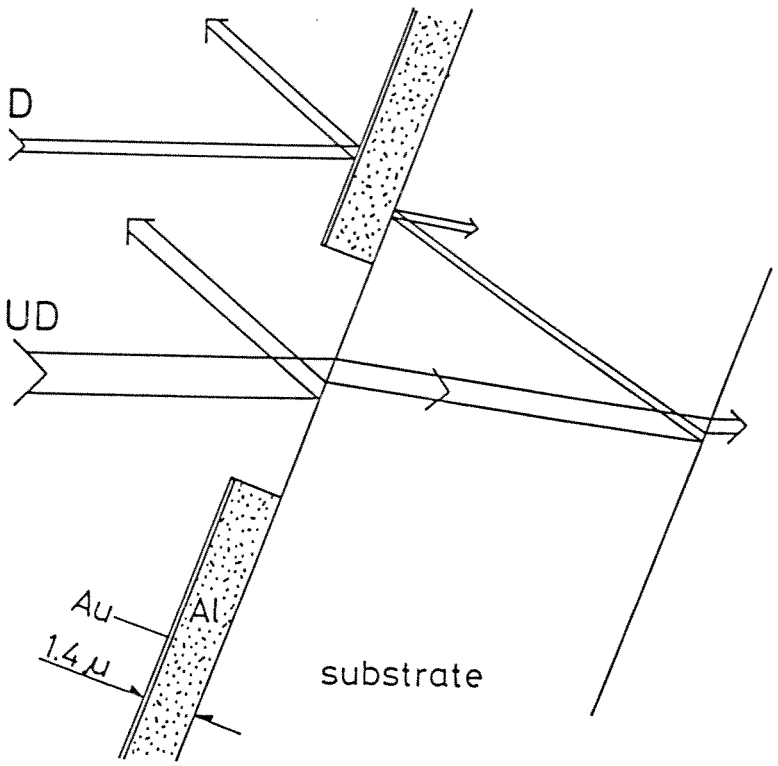

Fig. 5. Phase mirror UD: undiffracted light, D: diffracted light component.

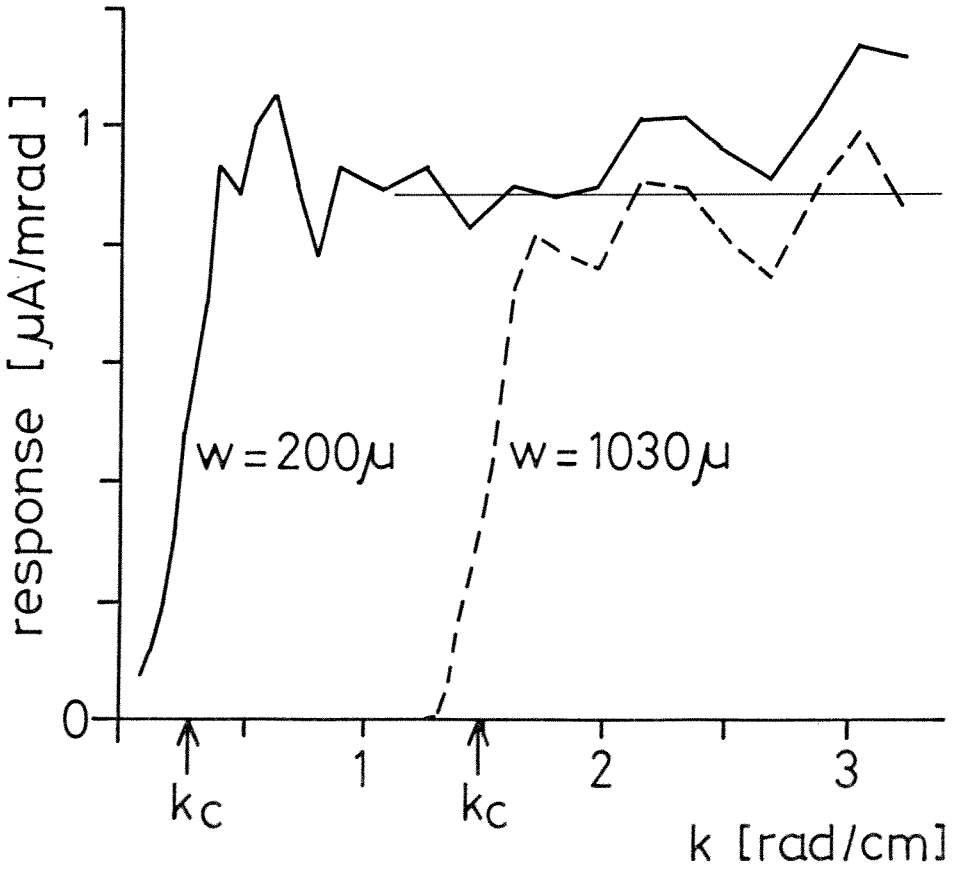

Fig. 6. Acoustic measurement of wavenumber responses.

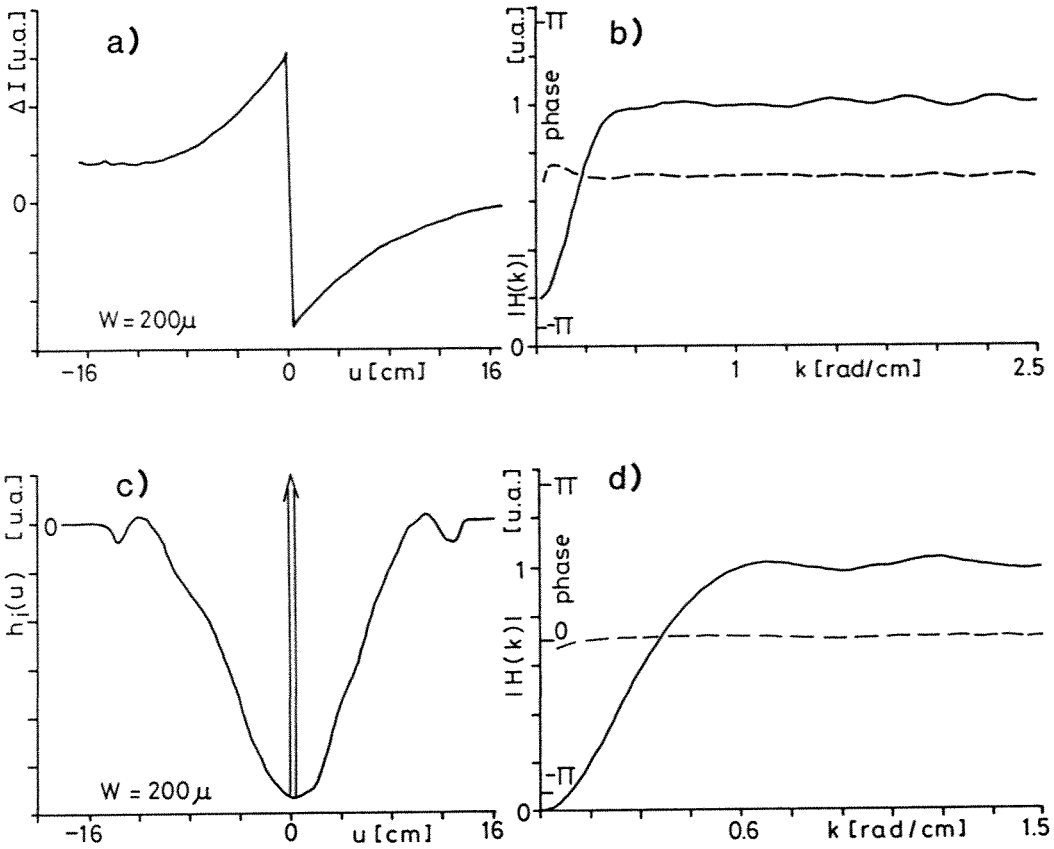

Fig. 7. Step and impulse response measurements
a) step response with w = 350 μ, b) corresponding transfer function
c) impulse response for w = 200 μ, d) transfer function

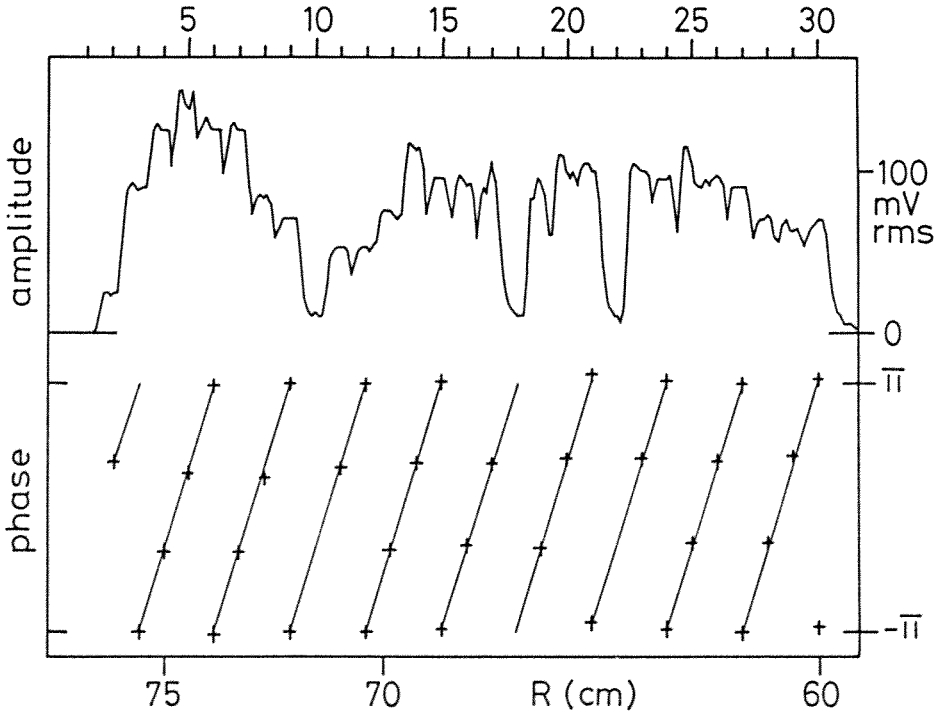

Fig. 8. Acoustic calibration signal from 20 kHz tweeter for the 30 element detector array.
a) amplitude as a function of element number/position, b) phase

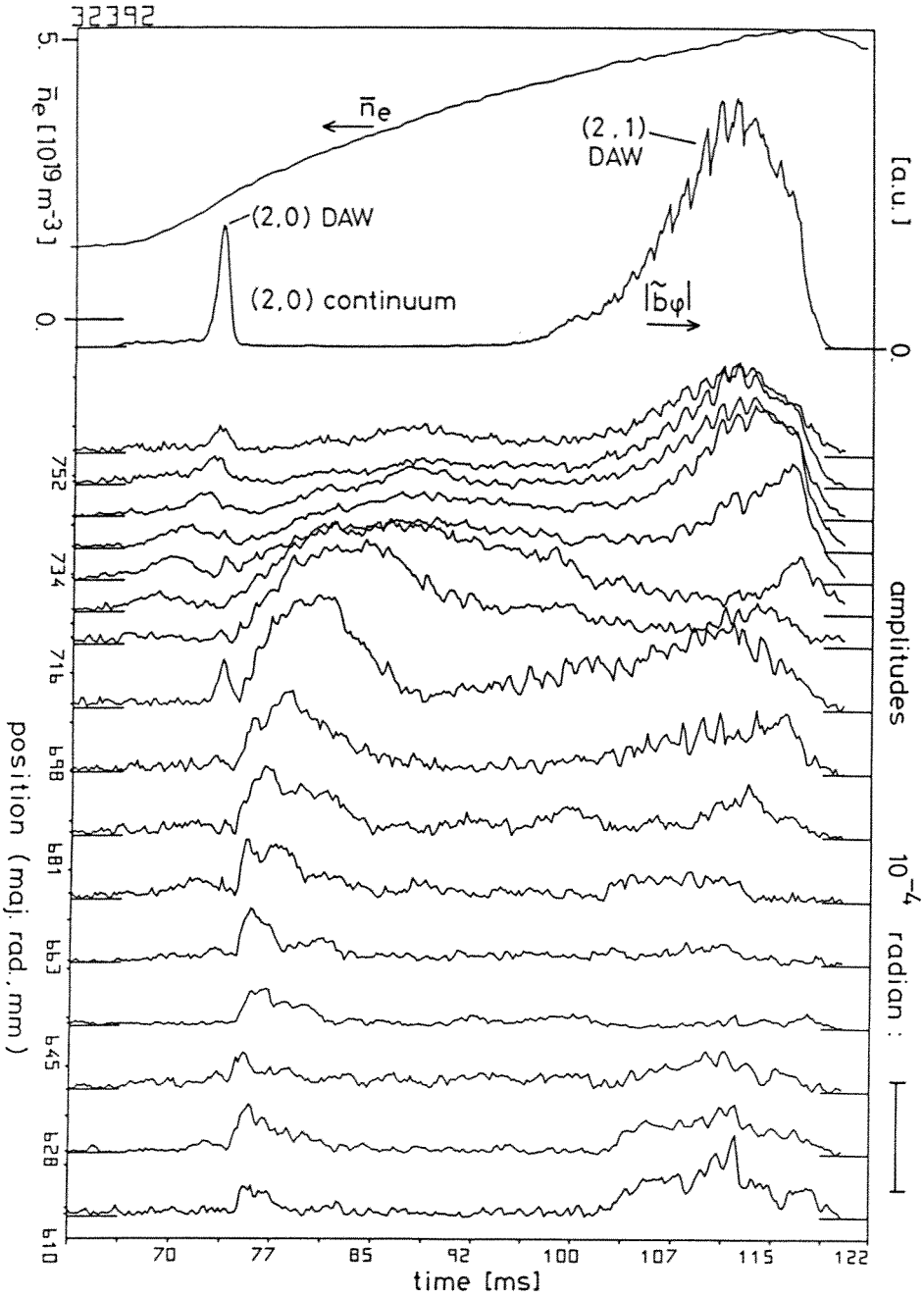

Fig. 9. Example of evolution of the synchronous density oscillation amplitude profile in an Alfvén Wave Heating discharge.

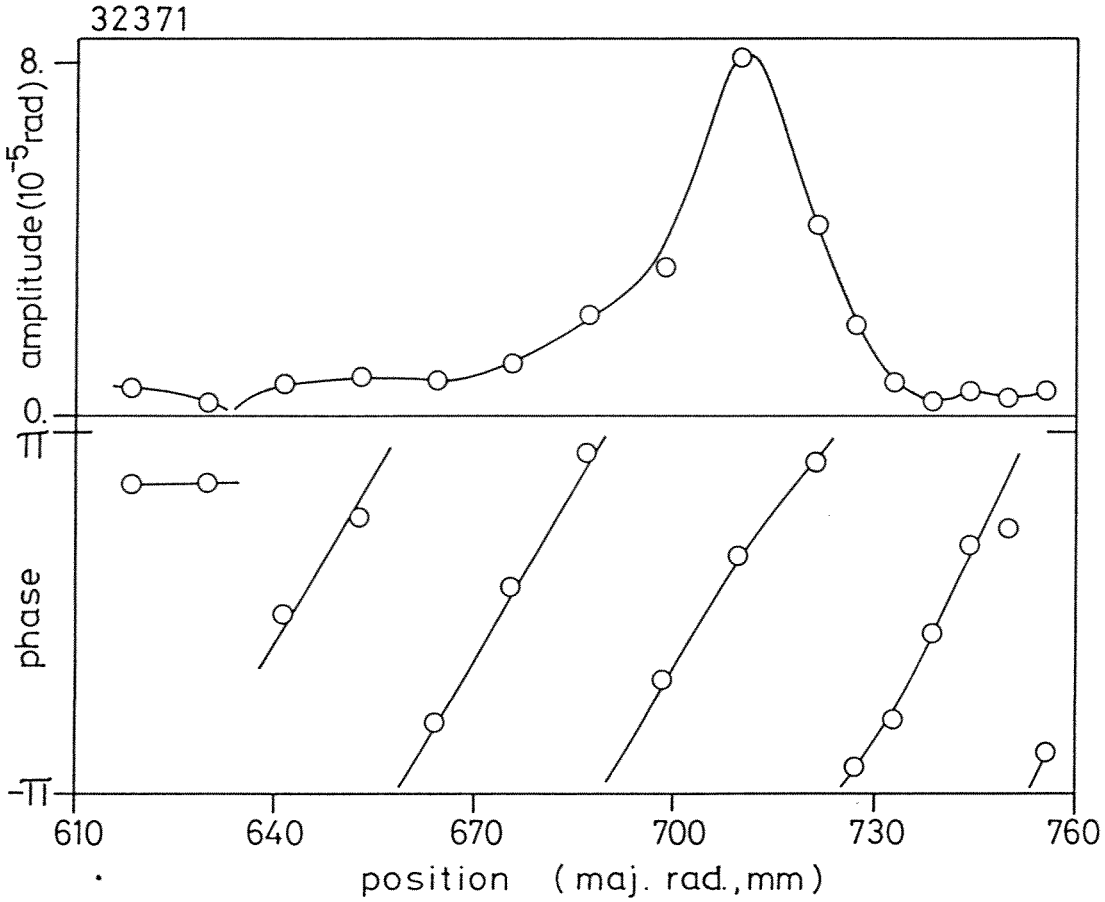

Fig. 10. Profile of amplitude and phase of synchronous density oscillations due to the kinetic Alfvén Wave, (2,0) continuum.

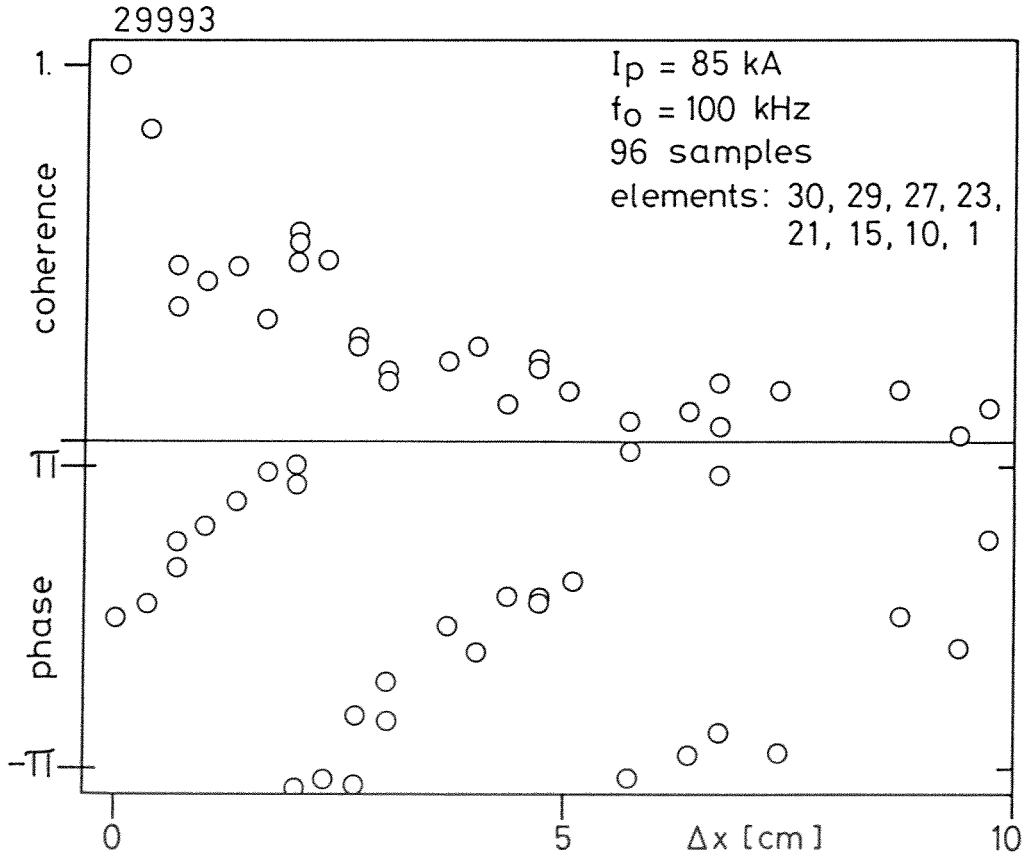

Fig. 11. Coherence and phase at 100 kHz as a function of detector separation for broadband turbulence in TCA.